BEST AVAILABLE IMAGES

Defective images within this document are accurate representations of the original documents submitted by the applicant.

Defects in the images may include (but are not limited to):

- BLACK BORDERS
- TEXT CUT OFF AT TOP, BOTTOM OR SIDES
- FADED TEXT
- ILLEGIBLE TEXT
- SKEWED/SLANTED IMAGES
- COLORED PHOTOS
- BLACK OR VERY BLACK AND WHITE DARK PHOTOS
- GRAY SCALE DOCUMENTS

IMAGES ARE BEST AVAILABLE COPY.

As rescanning documents *will not* correct images, please do not report the images to the Image Problem Mailbox.

Attorney's Docket No. 021238-478

IN THE UNITED STATES PATENT AND TRADEMARK OFFICE

In re Patent Application of	
Ping Li et al.	Group Art Unit: 1731
Application No.: 09/942,881	Examiner: Dionne A. Walls
Filed: August 31, 2001	Confirmation No.: 9479
For: OXIDANT/CATALYST NANOPARTICLES TO REDUCE CARBON MONOXIDE IN THE MAINSTREAM SMOKE OF A CIGARETTE	

DECLARATION UNDER 37 C.F.R. § 1.132 BY PING LI

Commissioner for Patents
P.O. Box 1450
Alexandria, VA 22313-1450

Sir:

I, Ping Li, hereby state as follows:

1. I am one of the inventors of the above-identified application.

2. I am familiar with the subject matter of the above-identified application. I am also familiar with the issues raised in the Office Action dated April 13, 2004. In the Office Action, the claims were rejected over U.S. Patent No. 4,397,321 ("Stuetz"). Based on the following experimental data which illustrates unexpected results of iron oxide nanoparticles for converting carbon monoxide to carbon dioxide, I respectfully but strongly disagree with the Examiner's conclusion.

3. The following standard Federal Trade Commission (FTC) method tests were conducted under my direction:

Experimental cigarettes were prepared with a mixture of 0.74 g of tobacco filler containing 80 mg of catalyst material comprised of iron oxide nanoparticles (specifically, NANOCAT™ Superfine iron oxide nanoparticles with an average particle size of about 3 nm according to the manufacturer Mach I Inc. of King of Prussia, Pennsylvania) supported on 1-3 μm Al_2O_3 (i.e., 30% iron oxide nanoparticles (about 24 mg of iron oxide nanoparticles) and 70% Al_2O_3 (about 56 mg of Al_2O_3)).

Control cigarettes were also prepared using the same types of cigarette components as the Experimental cigarettes, but without iron oxide nanoparticles or the Al_2O_3. The cigarettes

were prepared and tested according to the standard FTC method in a smoking machine. According to the standard FTC method, the cigarettes were subjected to a 35 ml, 2 second puff every minute, where the smoke was analyzed for determining reduction of carbon monoxide. The percentage carbon monoxide reduction set forth in the Table 1 was calculated by taking the difference in the average carbon monoxide level for the Control Average and the Experimental Average, then dividing the difference by the Control Average and multiplying the quotient by 100 for a percentage. Also, the results below were observed wherein RTD is Resistance To Draw in units of mm H_2O and PC is the puff count.

The results of Test 1 are as follows:

Test 1

Sample w/o Catalyst	RTD	Vent %	PC	TPM (mg)	CO_2 (mg)	CO (mg)	NO µg
Control 1	85	21	8	18.5	39.82	15.75	264.9
Control 2	103	14	8.2	16.9	37.17	15.02	244.5
Control 3	101	11	8	17.5	37.79	13.26	274.7
Control Average	96.3	15.3	8.1	17.6	38.3	14.7	261.4

Sample w/Catalyst	RTD	Vent %	PC	TPM (mg)	CO_2 (mg)	CO (mg)	NO µg	CO reduction
Experimental 1	121	13	7	8	31.64	9.26	195.6	
Experimental 2	113	14	7.1	7	29.55	7.57	167.4	
Experimental 3	128	13	7.7	8.9	33.62	9.25	198.4	
Experimental Average	120.7	13.3	7.3	8.0	31.5	8.7	187.1	41%

4. In another test conducted under my direction, carbon monoxide reduction was measured using the FTC method with control cigarettes (Sample 1), Al_2O_3 containing cigarettes (Sample 2) and iron oxide nanoparticle/Al_2O_3 containing cigarettes (Sample 3), wherein each of the cigarettes contained about 0.72 g of tobacco, the Al_2O_3 containing cigarette contained about 80 mg of Al_2O_3 and the iron oxide nanoparticle/Al_2O_3 containing cigarette contained about 80 mg of about 26 mg of iron oxide nanoparticles and about 54 mg of Al_2O_3. The percentage of carbon monoxide reduction is based upon the difference in carbon monoxide levels between Sample 1 and Sample 2 (or 3, respectively) divided by the carbon monoxide level of Sample 1, then multiplying the quotient by 100 for a percentage. The average results for five tested cigarettes for Samples 1-2 and three tested cigarettes for Sample 3 in Test 2 are as follows:

Test 2

Sample	CO (mg)	CO_2 (mg)	CO/CO_2	TPM (mg)	CO reduction
1	11.6	35.4	0.33	16.0	
2	10.9	34.6	0.31	12.9	6%
3	5.5	24.4	0.22	12.0	53%

5. The data from Tests 1 and 2 clearly show that a significantly lower amount of iron oxide nanoparticles achieves comparable carbon monoxide reduction compared to the much higher amount of colloidal manganese dioxide disclosed in Stuetz. Sample 2 shows that the effect of 80 mg of Al_2O_3 on carbon monoxide reduction (6%) is not significant compared to the 53% reduction using 80 mg of 26 mg iron oxide nanoparticles supported on 54 mg of Al_2O_3.

6. Also, I am familiar with iron oxide nanoparticles and believe that iron oxide nanoparticles were not commercially available prior to about the early 1990's. I have conducted searches for iron oxide nanoparticles using a search engine in the Philip Morris Technical Library, and the first published article discussing commercially available iron oxide nanoparticles that I found was "Structure and Dispersion of Iron-Based Catalysts for Direct Coal Liquefaction"

in Energy & Fuels, 1993, Vol. 7, pages 285-296 (Exhibit A), which discusses ultrafine iron-based direct coal liquefaction catalysts.

I hereby declare that all statements made herein of my own knowledge are true and that all statements made on information and belief are believed to be true; and further that these statements were made with the knowledge that willful false statements and the like so made are punishable by fine or imprisonment, or both, under Section 1001 of Title 18 of the United States Code and that such willful false statements may jeopardize the validity of the application or any patent issued thereon.

Date: 07/28/04

Ping Li

Structure and Dispersion of Iron-Based Catalysts for Direct Coal Liquefaction

G. P. Huffman,* B. Ganguly, Jianmin Zhao, K. R. P. M. Rao, N. Shah, Zhen Feng, F. E. Huggins, M. Mehdi Taghiei, and Fulong Lu

CFFLS, 233 Mining & Mineral Resources Bldg., University of Kentucky, Lexington, Kentucky 40506

I. Wender, V. R. Pradhan, and J. W. Tierney

Department of Chemical and Petroleum Engineering, University of Pittsburgh, Pittsburgh, Pennsylvania 15261

M. S. Seehra and M. M. Ibrahim

Physics Department, West Virginia University, Morgantown, West Virginia 26506

J. Shabtai and E. M. Eyring

Fuels Engineering and Chemistry Departments, University of Utah, Salt Lake City, Utah 84112

Received July 29, 1992. Revised Manuscript Received December 22, 1992

Mossbauer spectroscopy, XAFS spectroscopy, and a number of complementary techniques have been used to investigate the structure and size dispersion of a variety of ultrafine iron-based DCL catalysts. In the as-prepared state, iron that was chemically incorporated into the coal exhibited an FeOOH structure, while iron catalysts prepared separately had the Fe_2O_3 structure. The Mossbauer spectra exhibited pronounced superparamagnetic relaxation effects. The relaxation spectra could be analyzed at several temperatures to determine size distributions for the catalyst particles. The resulting size distributions were in the nanometer range and agreed reasonably well with size information obtained by SQUID magnetometry, STEM, and XRD. Radical structure functions (RSF) derived from the XAFS spectra of the catalysts confirmed the Mossbauer structural identifications and also exhibited significant size effects. While the interatomic distances determined from the RSF were close to those of the bulk phases, the coordination numbers of the iron neighbor shells were significantly decreased. The origins of this effect are (i) iron atoms on or near the surface of fine particles have fewer iron neighbors at distances of 3–4 Å and (ii) the electron mean free path is decreased for very small particles, causing an apparent decrease in coordination numbers. During DCL, the highly dispersed ferric iron rapidly reacts with H_2S to form pyrrhotite ($Fe_{1-x}S$). If insufficient sulfur is present in the reactor to convert all of the iron to pyrrhotite, the remainder is left in the form of a superparamagnetic oxide. An in situ XAFS study of the reactions of ultrafine Fe_2O_3 catalysts in a hydrogen donor solvent in the presence of elemental sulfur showed that conversion of a 30-Å catalyst to pyrrhotite proceeded fairly rapidly at 110–180 °C, while the transformation of an Fe_2O_3 catalyst of larger particle size (>100 Å) proceeded somewhat sluggishly at 250–320 °C.

Introduction

In recent years, there has been renewed interest in the use of iron-based catalysts for direct coal liquefaction (DCL). In part, this is because of obvious economical and environmental benefits. Iron is cheap and presents no environmental hazards; therefore, iron-based DCL catalysts can be used in a disposable mode. Additionally, a number of investigators have succeeded in producing iron DCL catalysts in very active, highly dispersed forms. Some of the methods used have included the use of oil-soluble iron compounds such as iron pentacarbonyl,[1,2] preparation of ultrafine ferric oxide and oxyhydroxide particles by a variety of chemical[3,4] and other methods,[5] chemical impregnation,[6–8] and cation exchange.[9–11] In most cases, the iron phases in the as-prepared or as-added form are not the active catalysts in DCL, but the catalyst precursors. For simplicity, however, we will simply use the term "catalyst" throughout.

(1) Suzuki, T.; Yamada, O.; Takehashi, Y.; Watanabe, Y. *Fuel Process. Technol.* 1985, *10*, 33–43.
(2) Herrick, D. E.; Tierney, J. W.; Wender, I.; Huffman, G. P.; Huggins, F. E. *Energy Fuels* 1991, *4*, 231–235.
(3) Tanabe, K.; Yamaguchi, T.; Hattori, H.; Sanada, Y.; Yokoyama, S. *Fuel Process. Technol.* 1984, *8*, 117–122.
(4) Pradhan, V. R.; Tierney, J. W.; Wender, I.; Huffman, G. P. *Energy Fuels* 1991, *5*, 497–507.
(5) "Nanocat" Superfine Iron Oxide, prepared by MACH I, Inc., 340 E. Church Rd., King of Prussia, PA 19406.
(6) Shabtai, J. S.; Saito, I. U.S. Patent, 4,728,418 (1988).
(7) Shabtai, J. S.; Zhang, Y. *Proc. 1989 Int. Conf. Coal Sci., Tokyo* 1989, *2*, 807–810.
(8) Shabtai, J. S.; Skulthai, T. *Proc. 1987 Int. Conf. Coal Sci., Maastricht, The Netherlands* 1987, 761–764.
(9) Cook, P. S.; Cashion, J. D. *Fuel* 1987, *66*, 661–668.
(10) Cook, P. S.; Cashion, J. D. *Fuel* 1987, *66*, 669–677.
(11) Huffman, G. P.; Ganguly, G.; Taghiei, M.; Huggins, F. E.; Shah, N. *Prepr. Pap.—Am. Chem. Soc., Div. Fuel Chem.* 1991, *36*(2), 561–569.

0887-0624/93/2507-0285$04.00/0

Discussions of the activity and product yields of the ultrafine iron-based DCL catalysts listed above have been given elsewhere[1-13] and will not be repeated here. Suffice it to say that they are highly active and appear to be competitive with more expensive nondisposable catalysts in terms of both total conversion and oil yields. The purpose of the present article is to discuss the structure and size dispersion of a variety of iron-based catalysts as determined primarily by two spectroscopic techniques; ^{57}Fe Mossbauer spectroscopy, and X-ray absorption fine structure (XAFS) spectroscopy. Complementary electron microscopy, SQUID magnetometry, and X-ray diffraction data are also discussed. For the most part, the catalysts discussed in this paper are those currently being investigated as part of the research program of the Consortium for Fossil Fuel Liquefaction Science (CFFLS).[2,4,6-8,11-13]

^{57}Fe Mossbauer spectroscopy has often been used to characterize iron-based DCL catalysts.[2,4,9-11,14-17] XAFS spectroscopy has become a powerful tool in catalysis science[18-21] and has been applied by several investigators to DCL catalysts.[4,11,19-21] Yamashita et al.[22] have conducted complementary Mossbauer and XAFS spectroscopy studies of iron-based gasification catalysts dispersed in coal. In some respects, these spectroscopic techniques are less direct than microscopic methods such as transmission electron microscopy (TEM). However, both methods offer the advantages of providing both structural and size sensitive information on the whole sample, and of comparatively simple sample preparation techniques.

Experimental Procedures

The samples investigated include sulfated Fe_2O_3 and FeOOH prepared by a process discussed in detail elsewhere,[4] iron chemically impregnated into several coals using a chemical treatment developed by Shabtai et al.[6-8] for a multistep liquefaction procedure, Fe_2O_3 precipitated on carbon black,[23] an ultrafine 30-Å Fe_2O_3 catalyst developed by Mach I,[5] iron incorporated into lignite by cation exchange,[11] and the derivatives of many of these species produced by hydrotreatment or DCL. Discussions of the synthesis of these catalysts may be found elsewhere.[1-13]

The Mossbauer spectrometer used in these experiments was a constant acceleration spectrometer of standard design.[24-26] The radioactive source consisted of 50–100 mCi of ^{57}Co in a Pd matrix. Sample cooling to temperatures as low as 10 K was achieved using an Air Products displex cryogenic system. The Mossbauer samples were in the form of powder samples mounted in Plexiglas compression holders.

The XAFS experiments were conducted at beamline X-19A at the National Synchrotron Light Source (NSLS) at Brookhaven National Laboratory. X-19A maintains the X-ray path from the synchrotron to the monochromator to the experimental hutch entirely in the storage ring vacuum in order to minimize beam absorption. Additionally, a helium pathway was maintained for the beam within the hutch, to further minimize unnecessary absorption by air. Electron currents in the ring were typically 100–200 mA. The X-ray energy was varied from approximately 100 eV below the Fe K-shell absorption edge to 800 eV above the edge using a double crystal Si(111) monochromator. Transmission XAFS measurements were conducted on concentrated catalyst samples, while fluorescent XAFS spectra were obtained from catalysts dispersed in coal or DCL residues using a Stearn-Heald type of detector.[27]

In situ XAFS measurements were carried out on two catalysts at temperatures up to 320 °C in a hydrogen donor (hexahydropyrene, HHP) containing elemental sulfur. These measurements used a hot cell designed by Lytle[28-30] which allows in situ fluorescent XAFS studies at elevated temperatures in user-selected environments.

Results and Discussion

1. Mossbauer Spectroscopy Results. Typical Mossbauer spectra of the as-prepared or as-dispersed catalysts are shown in Figures 1 and 2. Figure 1 shows the room temperature and 12 K spectra of a sulfated Fe_2O_3 catalyst,[4] while Figure 2 shows the 12 K spectrum of a lignite (PSU sample 1482, Hagel seam) loaded with iron by cation exchange[11] and the 12 K spectra of a Wyodak subbituminous coal impreganted with iron and subjected to a mild hydrotreatment (290 °C, 1000 psig of H_2) in the multistep liquefaction procedure developed by Shabtai and co-workers.[6-8] The Mossbauer parameters measured at room temperature and at 12 K for these and all other samples investigated in this study are summarized in Table I. In general, they are typical of either superparamagnetic Fe_2O_3 or FeOOH. Figure 1 is typical of samples investigated in this study which have the Fe_2O_3 structure, while Figure 2 is typical of samples which exhibited an FeOOH type of structure.

In all cases, the Mossbauer spectra are typical of superparamagnetic materials. That is, α-Fe_2O_3 and the most common iron oxyhydroxide, α-FeOOH, are both antiferromagnetic with Neel temperatures substantially above room temperature and would exhibit only six-peak magnetic hyperfine spectra at room and lower temperatures in their bulk form. For the current samples, however, the particles are small enough to behave superparamagnetically,[31,32] which causes rapid relaxation of the particle

(12) Huffman, G. P.; Huggins, F. E.; Ganguly, B.; Shah, N.; Taghiei, M. M.; Hager, G. T. *Proceedings, 1991 International Conference on Coal Science, Newcastle, England*; Butterworth-Heineman Ltd.: London, 1991; pp 826–829.

(13) *Cooperative Research in Coal Liquefaction.* Annual Report (5/1/90–4/30/91) on DOE Contract No. DE-FC22-89PC89851, February 15, 1992.

(14) Montano, P. A.; Granoff, B. *Fuel* **1980**, *59*, 214.

(15) Montano, P. A.; Bommannavar, A. S.; Shah, V. *Fuel* **1981**, *60*, 703.

(16) Bommannavar, A. S.; Montano, P. A. *Fuel* **1982**, *61*, 523.

(17) Ogawa, T.; Stenberg, V. I.; Montano, P. A. *Fuel* **1984**, *63*, 1660–1663.

(18) Lytle, F. W.; Via, G. H.; Sinfelt, J. H. In *Synchrotron Radiation Research*; Winick, H., Doniach, S., Eds.; Plenum Press: New York, 1980; pp 401–424.

(19) Prins, R.; Koningsberger, D. C. Catalysis. In *X-Ray Absorption: Principles, Applications, Techniques of EXAFS, SEXAFS and XANES*; Koningsberger, D. C., Prins, R., Eds.; John Wiley & Son: New York, 1988; Chapter 8, pp 321–372.

(20) Clausen, B. S.; Topsoe, H.; Candia, R. *J. Phys. Chem.* **1981**, *85*, 3868.

(21) Bouwens, S. M. A. M.; van Veen, J. A. R.; Koningberger, D. C.; de Beer, V. H. J.; Prins, R. *J. Phys. Chem.* **1991**, *95*, 123–134.

(22) Yamashita, H.; Oktsuka, Y.; Yoshida, S.; Tomita, A. *Energy Fuels* **1989**, *3*, 686.

(23) Sample provided by Malvina Farcasiu, U.S. DOE Pittsburgh Energy Technology Center, Pittsburgh, PA.

(24) Huffman, G. P.; Huggins, F. E. *Fuel* **1978**, *47*, 592–604.

(25) Huggins, F. E.; Huffman, G. P. Mossbauer Analysis of the Iron-Bearing Phases in Coal, Coke, and Ash. In *Analytical Methods for Coal and Coal Products*; Karr, Jr., C., Ed.; Academic Press: New York, 1979; Vol. III pp 371–423.

(26) Huffman, G. P. *CHEMTECH* **1980**, *10*, 504–511.

(27) Lytle, F. W.; Greegor, R. B.; Sandstrom, D. R.; Marque, E. C.; Wong, Joe; Sprio, C. L.; Huffman, G. P.; Huggins, F. E. *Nucl. Instrum. Methods* **1984**, *226*, 542–548.

(28) Sinfelt, J. H.; Via, G. H.; Lytle, F. W. *J. Chem. Phys.* **1982**, *76*, 2779.

(29) Huggins, F. E.; Shah, N.; Huffman, G. P.; Lytle, F. W.; Greegor, R. B.; Jenkins, R. G. *Fuel* **1988**, *67*, 1662–1667.

(30) Taghiei, M. M.; Huggins, F. E.; Shah, N.; Huffman, G. P. *Energy Fuels*, in press.

(31) Neel, L. *Rev. Mod. Phys.* **1953**, *25*, 293.

(32) Brown, W. F. *Phys. Rev.* **1963**, *130*, 1677.

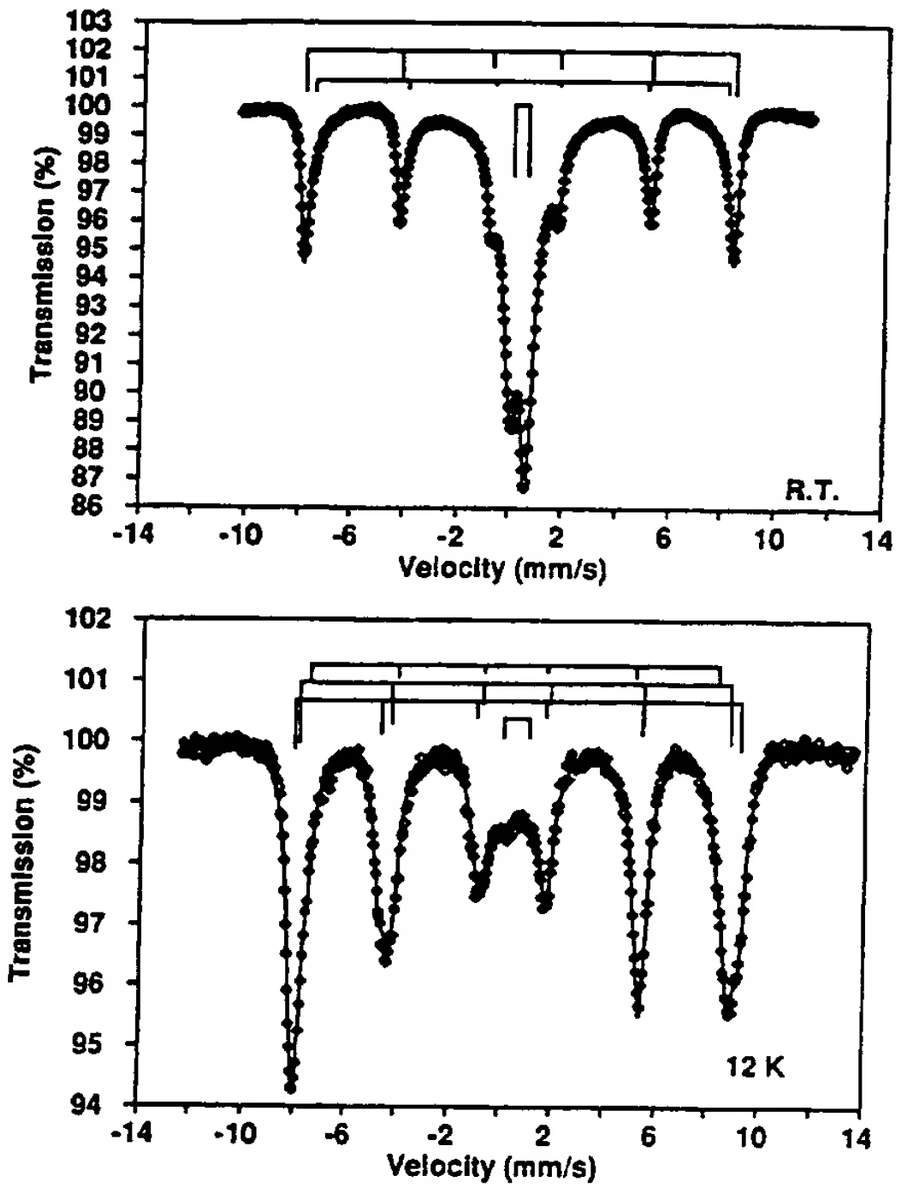

Figure 1. Room temperature and 12 K spectra obtained from an Fe_2O_3/SO_4 catalyst.

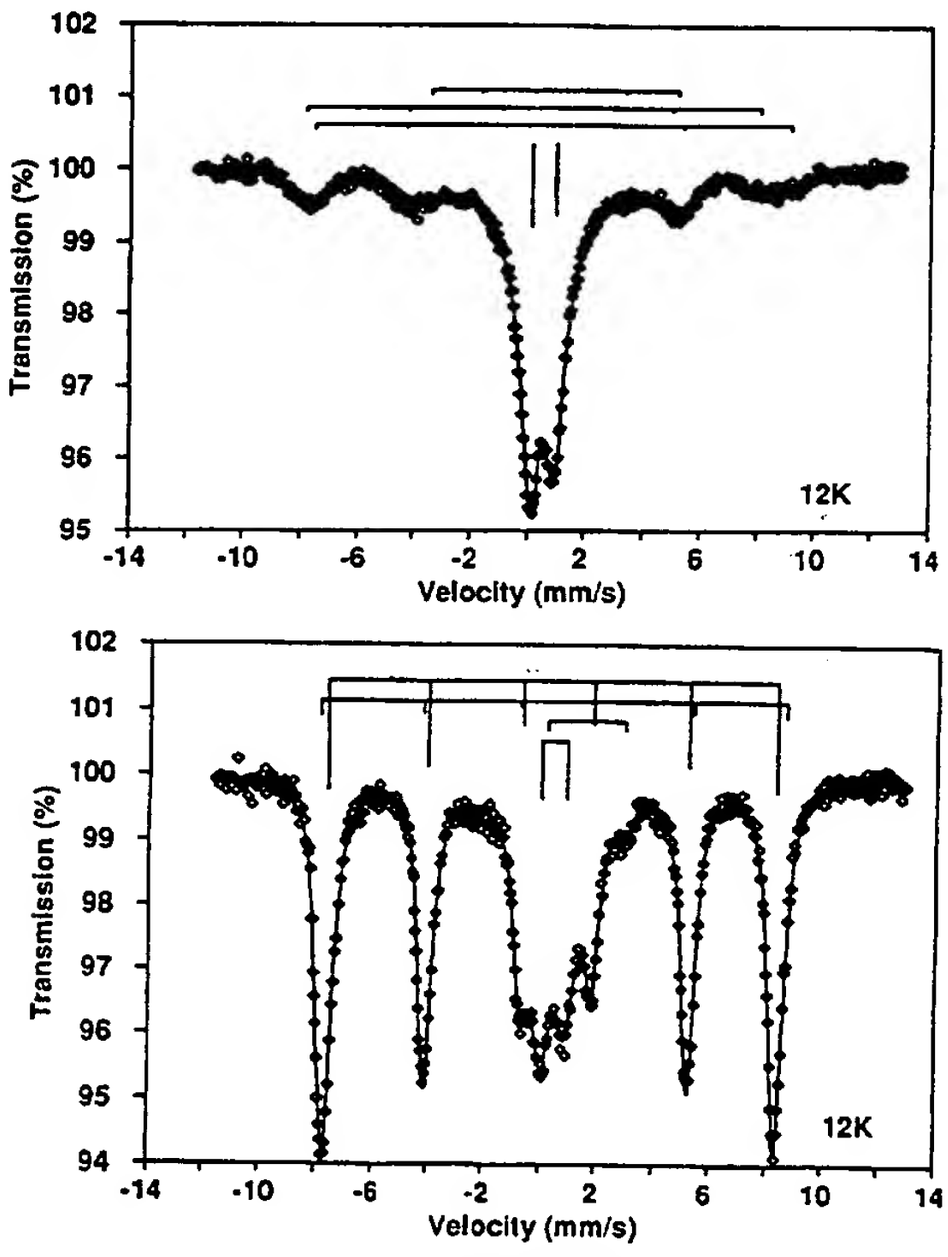

Figure 2. Mossbauer spectra obtained at 12 K from a chemically impregnated and hydrotreated ($FeCl_3$-$6H_2O$, upper spectrum) and a cation-exchanged lignite (Fe acetate, lower spectrum).

spin systems, resulting in spin relaxation effects[33,34] that give rise to spectra that are a superposition of broadened magnetic hyperfine and quadrupole (doublet or two peak) spectra. As discussed in numerous references dealing with Mossbauer studies of superparamagnetic materials,[33-42] the frequency, f, with which the coupled spins of a particle change direction is given by

$$f = f_0 \exp\{-K_a V/kT\} \quad (1)$$

where K_a is the magnetic anisotropy constant, V is the particle volume, f_0 is a constant frequency factor, k is the Boltzman constant, and T is the temperature. When the frequency f is less than the nuclear Larmor frequency, f_L, of the ^{57}Fe nucleus, the particle will exhibit a six-peak magnetic hyperfine pattern. When $f > f_L$, rapid spin relaxation causes the spectrum to gradually collapse into a quadrupole doublet. To a first approximation, one can define a critical particle volume, V_c, above which a particle will exhibit a magnetic hyperfine spectrum. At temperature T, V_c is given by

$$V_c = kT \ln\{f_0/f_L\}/K_a \quad (2)$$

Using the theoretical expressions for Mossbauer spectra given by Wickmann,[33] the validity of this approximation can be examined. The results for α-Fe_2O_3 are shown in Figure 3. Here, we have used the value of the magnetic anisotropy constant given by van der Kraan[36] (0.55×10^5 J/m^3) and have calculated f_L from the expression

$$f_L = g\beta H_0/h \quad (3)$$

where g and β are the nuclear g value and Bohr magneton, h is the Planck constant, and H_0 is the magnetic hyperfine field of bulk α-Fe_2O_3 (515 kG at room temperature). Various authors[33-42] have used a range of values (10^9–10^{12} s^{-1}) for the constant frequency parameter, f_0. As discussed in two forthcoming publications,[43,44] we have adopted an empirical approach. The Mossbauer spectrum at 10 K was obtained from an iron oxide (FeOOH structure) catalyst provided by Mach I, Inc.[5] that consisted of approximately spherical particles with a narrow size distribution and an average particle diameter of 32 Å.[45] The spectrum was fit using a superparamagnetic relaxation model[33,43] and gave a relaxation time of 10^{-7} s ($f = 10^7$ s^{-1}). Insertion of this value and the particle volume for 32-Å particles into eq 1 gave a value of 10^{12} s^{-1} for f_0, which was used for the analysis of all spectra obtained in this study.

Using these values of f_0, f_L, and K_a, and assuming spherical particles, a critical diameter, $d_c = 118$ Å is derived

(33) Wickman, H. H. In *Mössbauer Effect Methodology*; Gruverman, I. J., Ed.; Plenum Press: New York, 1966; Vol. 2.
(34) van der Woude, F.; Dekker, A. J. *Phys. Status Solidi* **1965**, *9*, 775; **1966**, *13*, 181.
(35) Kundig, W.; Bömmel, H.; Constabaris, G.; Lindquist, R. H. *Phys. Rev.* **1966**, *142*, 327.
(36) van der Kraan, A. M. *Phys. Status Solidi* **1973**, *18*, 215; Thesis, 1972.
(37) Morup, S.; Dumesic, J. A.; Topsoe, H. In *Applications of Mossbauer Spectroscopy*; Cohen, R. L., Ed.; Academic Press: New York, 1980; Vol. 2, p 1.
(38) Krop, K.; Korecki, J.; Zukrowski, J.; Karas, W. *Int. J. Magn.* **1974**, *6*, 19–23.
(39) Dehner, H. L.; Ritter, G.; Wegener, H. H. F. *Phys. Lett.* **1974**, *46A*, No. 5, 333–335.
(40) Belozerskii, G. N.; Pavlyukhin, Yu. T. *Sov. Phys. Solid State* **1977**, *19*, No. 5, 745–750.
(41) Van der Kraan, A. M. Thesis, 1972.
(42) Rodmacq, B. *J. Phys. Chem. Solids* **1984**, *45*, No. 11/12, 1119–1127.
(43) Ganguly, B.; Rao, K. R. P. M.; Huggins, F. E.; Shah, N.; Huffman, G. P. Determination of Iron Oxide Catalyst Size Distributions from Superparamagnetic Mossbauer Relaxation Spectra, *J. Catal.*, in press.
(44) Ganguly, B.; Huggins, F. E.; Rao, K. R. P. M.; Zhao, J.; Huffman, G. P. Anomalous Recoilles Fraction of 30 Å FeOOH Particles, submitted to *Phys. Rev. B.*
(45) Feng, Z.; Huggins, F. E.; Zhao, J.; Huffman, G. P. Transmission Electron Microscopy Studies of the Size and Structure of an Ultrafine Iron Oxide Catalyst, submitted to the *J. Catal.*

Table I. Mössbauer Parameters and Iron Percentages for Each Iron Type Observed[a]

sample	T (K)	phase[b]	H	IS	QS	% Fe
Fe_2O_3 on carbon black	295	para/sp Fe_2O_3		0.35	0.58	52
		mag Fe_2O_3	499	0.38	−0.11	23
		spm Fe_2O_3	500	0.42	−0.12	25
Fe_2O_3 on carbon black	12	para/sp Fe_2O_3		0.31		5
		mag Fe_2O_3	528	0.49	−0.10	58
		mag Fe_2O_3	500	0.47	−0.05	16
		mag Fe_2O_3	457	0.40	−0.02	21
Fe_2O_3/SO_4 (6.1% SO_4)	295	para/sp Fe_2O_3		0.40	0.68	45
		mag Fe_2O_3	501	0.41	−0.12	35
		spm Fe_2O_3	503	0.40	−0.10	20
Fe_2O_3/SO_4 (6.1% SO_4)	12	para/sp Fe_2O_3		0.56	1.00	10
		mag Fe_2O_3	537	0.45	0.10	34
		mag Fe_2O_3	519	0.49	−0.07	43
		mag Fe_2O_3	491	0.45	−0.04	13
Fe_2O_3/SO_4 (3.4% SO_4)	295	para/sp Fe_2O_3		0.50	1.3	6
		mag Fe_2O_3	501	0.36	−0.11	51
		mag Fe_2O_3	479	0.36	−0.12	17
		mag Fe_2O_3	446	0.33	−0.14	26
Fe_2O_3/SO_4 (2.1% SO_4)	295	para/sp Fe_2O_3		0.39	0.58	25
		mag Fe_2O_3	496	0.37	−0.11	26
		mag Fe_2O_3	471	0.36	−0.09	29
		spm Fe_2O_3	480	0.35	−0.10	20
Fe_2O_3/SO_4 (2.1% SO_4)	12	para/sp Fe_2O_3		0.30		2
		mag Fe_2O_3	527	0.47	−0.12	92
		mag Fe_2O_3	506	0.22		6
FeOOH/SO_4 (3.4% SO_4)	295	para/sp FeOOH		0.36	0.53	52
				0.35	0.84	36
		para/sp FeOOH		0.35	1.24	12
FeOOH/SO_4 (3.4% SO_4)	12	mag FeOOH	496	0.51	−0.08	46
		mag FeOOH	462	0.51	−0.06	25
		mag FeOOH	437	0.49	−0.05	20
		mag FeOOH	402	0.51	−0.01	9
C.E[c] lignite $FeCl_2$ soln	295	para/sp FeOOH		0.27	0.65	100
C.E.[c] lignite $FeCl_2$ soln	12	para/sp FeOOH		0.54	0.77	58
		mag FeOOH	544	0.57	0.10	42
C.E.[c] lignite Fe acetate soln	295	para/sp FeOOH		0.42	0.79	10
		para/sp FeOOH		0.57	1.29	6
		mag FeOOH	326	0.36	−0.10	34
		mag FeOOH	266	0.37	−0.10	16
		spm FeOOH	325	0.40	−0.12	34
C.E.[c] lignite Fe acetate soln	12	para/sp FeOOH		0.44	0.89	29
		mag FeOOH	514	0.43	−0.10	6
		mag FeOOH	497	0.44	−0.12	65
C.I.[d] Wyodak Coal	295	para/sp FeOOH		0.26	0.66	22
		para/sp FeOOH		0.37	0.87	71
		siderite		1.13	1.92	8
C.I.[d] Wyodak coal	12	para/sp FeOOH		0.53	0.86	81
		mag FeOOH	526	0.42	0.09	7
		mag FeOOH	477	0.48	−0.21	8
		spm FeOOH	500	0.47	0.09	4
C.I.[d] Wyodak coal after HT at 270 °C	295	para/sp FeOOH		0.39	0.79	89
		Fe^{2+}		0.89	2.44	4
		mag FeOOH	203	0.25	−0.02	7
C.I.[d] Wyodak coal after HT at 270 °C	12	para/sp FeOOH		0.54	0.79	25
		para/sp FeOOH		0.57	1.39	15
		mag FeOOH	491	0.55	−0.01	23
		mag FeOOH	463	0.50	−0.18	9
		spm FeOOH	500	0.40	−0.12	28
C.I.[d] Blind Canyon coal	295	para/sp FeOOH		0.37	0.68	85
		siderite		1.16	1.96	15
C.I.[d] Blind Canyon coal	12	para/sp FeOOH		0.44	0.72	51
		para/sp FeOOH		0.59	1.02	7
		siderite		1.39	2.62	10
		mag FeOOH	469	0.48	−0.12	32
C.I.[d] Blind Canyon coal after HT at 270 °C	295	para/sp FeOOH		0.37	0.56	64
		para/sp FeOOH		0.37	0.95	36
C.I.[d] Blind Canyon coal after HT at 270 °C	12	para/sp FeOOH		0.36	1.22	22
		para/sp FeOOH		0.31		13
		siderite		1.18	2.86	9
		mag. FeOOH	483	0.51	0.03	23
		mag. FeOOH	478	0.50	−0.19	24
		mag. FeOOH	455	0.43	−0.19	9

[a] Hyperfine field H (kilogauss); isomer shift, IS (mm/s); quadrupole splitting, QS (mm/s). The approximate percentage error in the reported values is 5%. [b] For superparamagnetic phases, the iron contributing primarily to the nonmagnetic quadrupole peaks is denoted as "para/sp", while that contributing to the magnetic hyperfine pattern is denoted as "mag". [c] Cation-exchanged, demineralized, lignite (PSOC 1482). [d] Chemically impregnated via the Shabtai method.[6-8]

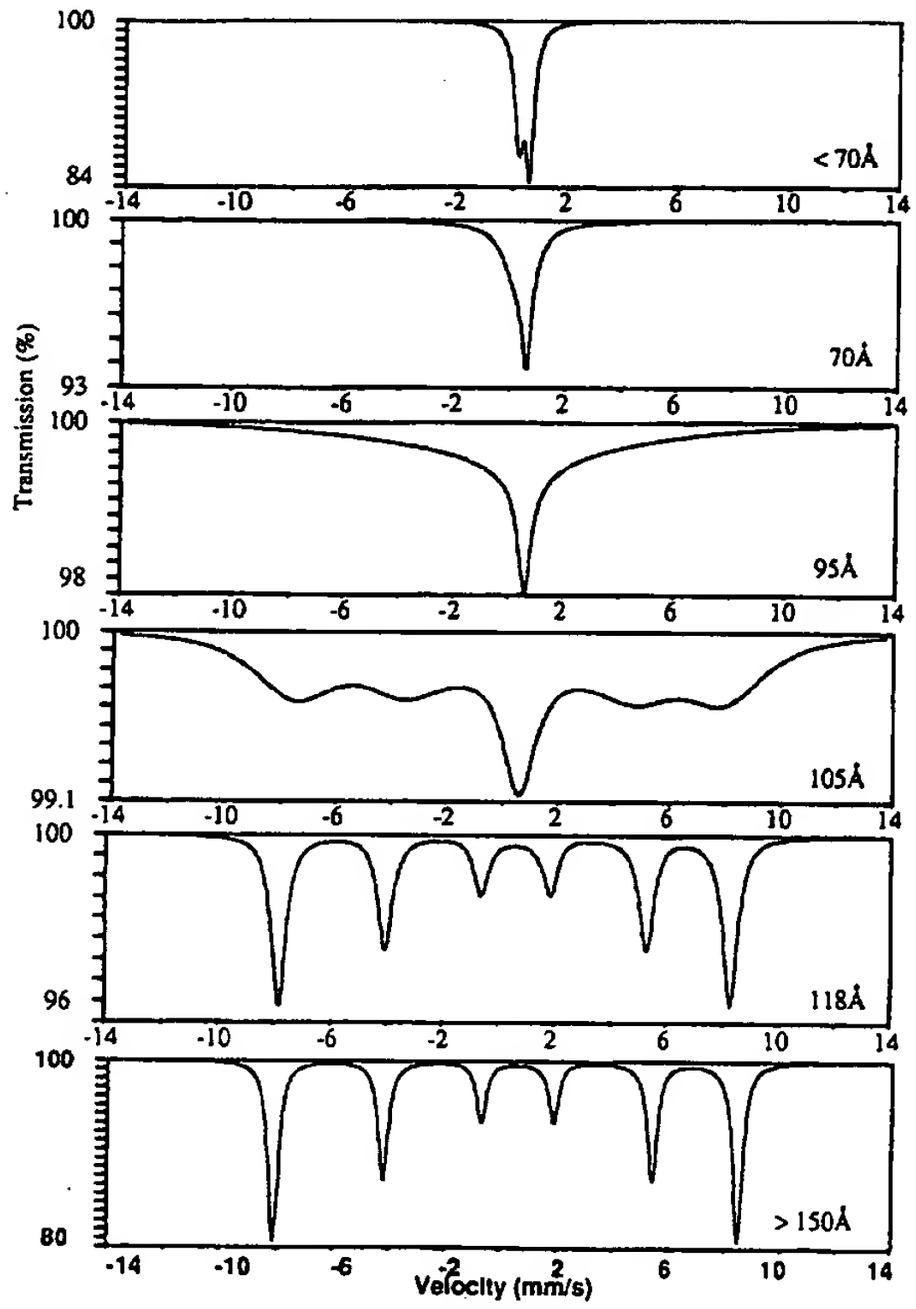

Figure 3. Theoretical plots of relaxation spectra of Fe_2O_3 at room temperature as a function of particle size.

for Fe_2O_3 at 295 K. It is seen in Figure 3 that the theoretical spectrum is indeed a six-peak magnetic hyperfine spectrum at this particle diameter, although it is slightly broadened. At a somewhat larger particle diameter, a sharp six-line magnetic hyperfine pattern with no significant broadening is seen.

For particles with diameters less than the critical diameter, Figure 3 shows that the collapse to a quadrupole doublet occurs gradually with decreasing particle size. It is seen that a sequence of markedly broadened relaxation spectra occurs as the particle size decreases below the critical diameter of 118 Å. At a diameter slightly below 70 Å, a pattern that could properly be called a broadened, asymmetric, quadrupole doublet emerges.

These results lead us to a simple method for deducing approximate size distributions for the as-prepared/dispersed catalysts. The spectra are least-squares analyzed using a model that includes one or several broadened magnetic hyperfine spectra and quadrupole doublets and a superparamagnetic relaxation spectrum based on the theoretical models given in the literature.[33,34] For the superparamagnetic component, it is assumed that either α-Fe_2O_3 or α-FeOOH is the correct structure insofar as the bulk material Mossbauer parameters are concerned, and the only variables for this component are the mean relaxation time and the relative amplitude. The use of this approximation for treating the often complex spectra exhibited by superparamagnetic iron-based catalysts will be discussed in more detail elsewhere.[43] For the purposes of the current paper, it is sufficient to note that the percentage of iron contributing to the magnetic hyperfine components should be approximately equal to the percentage of iron contained in particles of volume greater than the critical volume, V_c, given by eq 2.

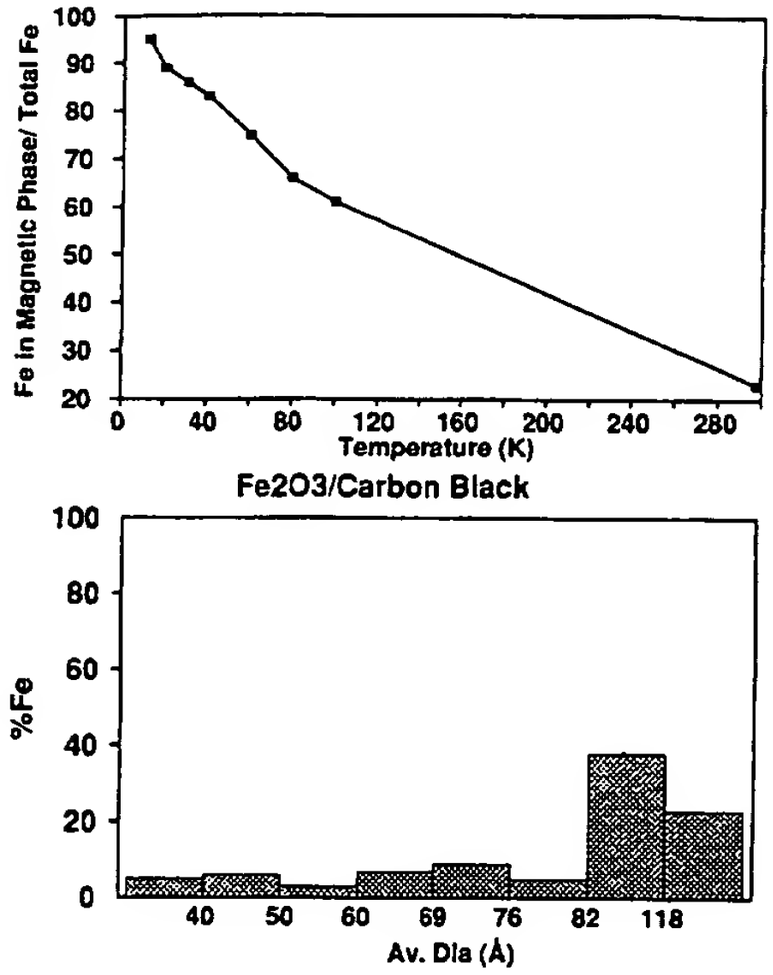

Figure 4. Magnetic percentage vs temperature for Fe_2O_3 on carbon black and resulting size distributions.

Clearly, there is some ambiguity with this approximation. For particles that are only a few nanometers in diameter, there will always be several magnetic components due to the fact that iron spins on or near the particle surface are exchange-coupled to less neighboring iron spins than those in the interior of the particles. The interior iron atoms will therefore exhibit hyperfine fields closer to the bulk value than the surface atoms. For iron chemically impregnated or cation exchanged into the coal, there may be several inequivalent atomic environments for the iron contributing to the magnetic hyperfine spectra. Additionally, there will be other iron-bearing species present in the coal, several of which (siderite, szomolnokite, jarosite) are magnetically ordered at low temperatures. All of these factors complicate the spectra and make it somewhat more difficult to accurately derive the correct magnetic percentage to be used in conjunction with eq 2 to determine size distributions. Nevertheless, the derived percentages are believed to have an error of not more than 10–20% of their true values.

The results obtained using this approach for the Fe_2O_3 on carbon black catalyst are shown in Figure 4. The top half of Figure 4 shows the Mossbauer magnetic percentage for this catalyst as a function of temperature. Then, using eq 2 and assuming spherical particles, a critical diameter can be derived for each temperature, leading to the size distribution in the bottom half of Figure 4. Similar size distributions are shown for a number of as-prepared or as-dispersed catalysts in Figure 5. Note that the horizontal axes in Figures 4 and 5 are not linear but are divided into equal increments demarked by the critical particle diameter for each temperature (eq 2). These results were again derived using eq 2 and the magnetic anisotropy constants for α-FeOOH given by Rodmacq[42] (1.67×10^5 J/m^3) and for α-Fe_2O_3 by van der Kraan[36] (0.55×10^5 J/m^3). For many of these samples, Mossbauer measurements have been made at only a few temperatures, leading to relatively coarse size distributions. Furthermore, it is known from TEM measurements[4,45] that these catalyst particles are not spherical. For the Fe_2O_3 samples, the particles range from oblate spheroids to somewhat tabular shapes, as illustrated by the TEM micrograph shown in

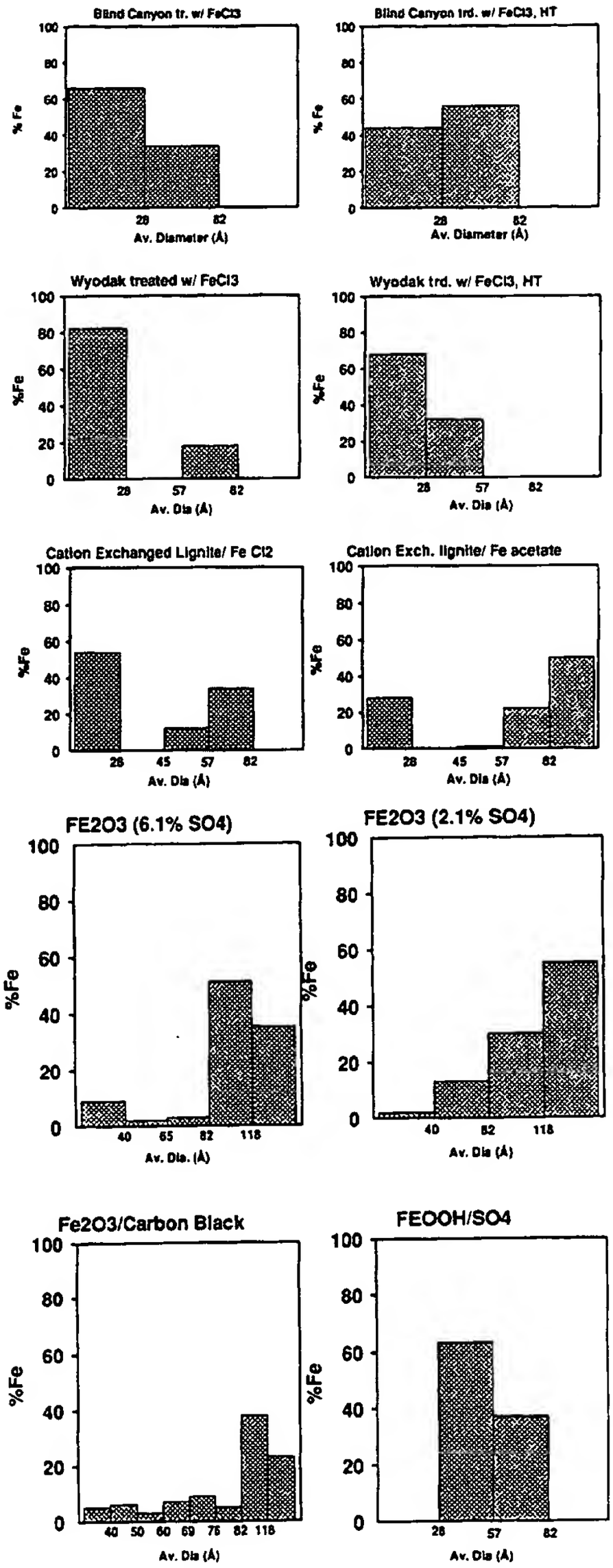

Figure 5. (a, top) Size distribution for catalysts chemically impregnated into coal determined from spm Mossbauer spectra. (b, bottom) Size distributions for as-prepared iron oxide catalysts determined from spm Mossbauer spectra.

Figure 6a, while the FeOOH particles are often more elongated.[4] Nevertheless, size distributions such as those shown in Figures 4 and 5 are very useful for comparing the relative dispersion of such catalysts, with the derived "diameter" viewed as a dimension characteristic of the particle size. Furthermore, it is worth noting that mean diameters and size distributions derived by other methods such as X-ray diffraction (XRD) line broadening[4] and magnetic measurements[46] are subject to the same reservations and limitations.

(46) Ibrahim, M. M.; Zhao, J. Seehra, M. S. *J. Mater. Res.* **1992**, *7*, 1856–1860.

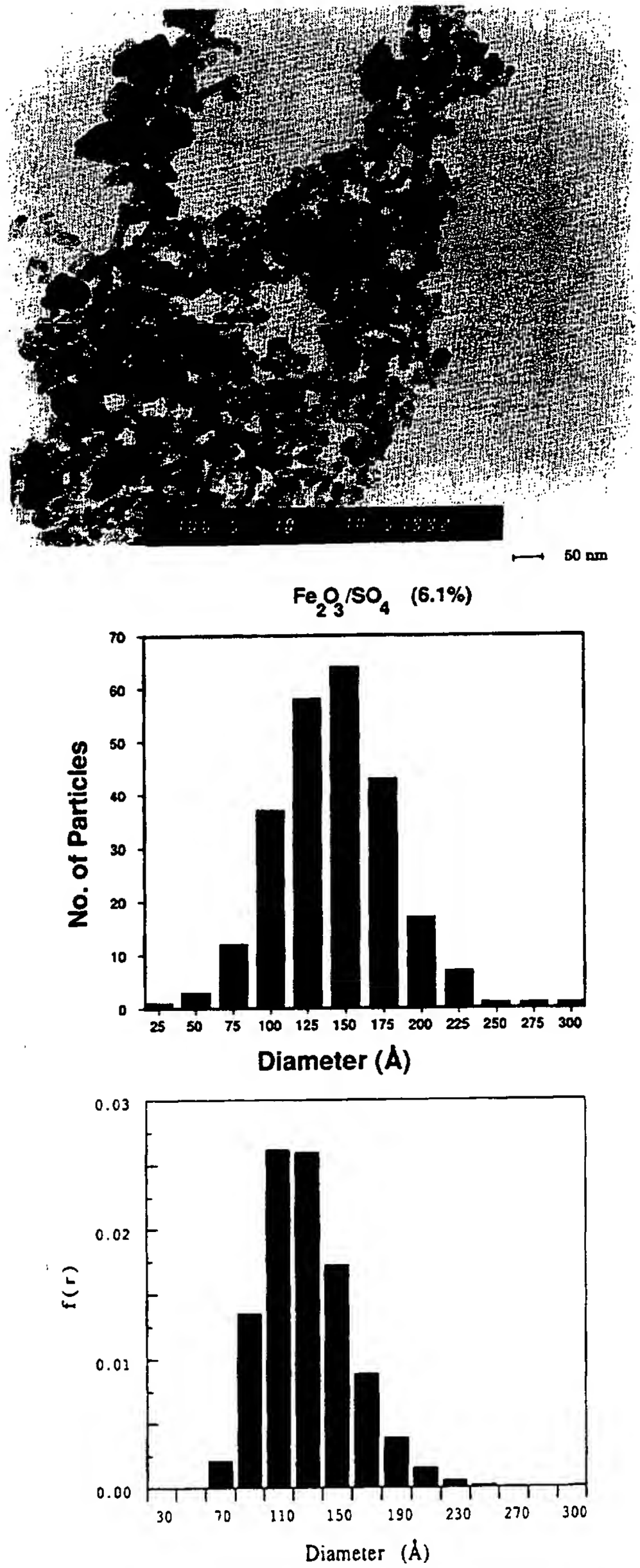

Figure 6. (a, top) TEM micrograph of a sulfated Fe_2O_3 catalyst (6.1% SO_4). (b, middle) Size distribution determined from TEM micrographs of a sulfated Fe_2O_3 catalyst (6.1% SO_4). (c, bottom) Size distribution for Fe_2O_3/SO_4 (6.1%) determined from SQUID magnetometry.

It is of interest to compare the particle sizes of catalysts prepared by different methods. It is noted that the specimens prepared by chemical incorporation of the iron into the coal, which have an FeOOH type of structure, exhibit smaller sizes than the catalysts of Fe_2O_3 structure. From Figure 5a, it is seen that the mean dimension characteristic of most of the iron incorporated into Blind Canyon and Wyodak coal by the Shabtai treatment[6–8] is

less than 28 Å, suggesting that much of this iron may be molecularly dispersed in the coal. These coals were impreganted using the aqua complex, $Fe(H_2O)_6Cl_3$, in which the Fe ion is coordinated by six water ligands. This structure should be quite stable and resistant to agglomeration up to about 250 °C. The polarizing coal medium may cause dissociation of some water ligands, yielding an FeOOH structure which is partially hydrated and resists agglomeration. During the initial mild hydrotreatment (290 °C, 1000 psi of H_2) of the Shabtai multistep treatment, it is seen that a small amount of agglomeration and growth of the catalyst particles occurs, but the basic FeOOH structure is unchanged. It is believed that the iron acts as a hydrogenolytic bond cleavage catalyst during this step.[6-8] Again referring to Figure 5a, it appears that much of the iron introduced into lignite by cation exchange may also be molecularly dispersed. Additionally, these size distributions appear to have a bimodal character. Consequently, it does not appear that simple size distribution models such as the often utilized log normal distribution[47] are appropriate for these samples.

In the case of the sulfated Fe_2O_3 catalysts, XRD, TEM, and SQUID magnometry data on the particle sizes are also available.[4,45,46] For the sample containing 6.1% SO_4^{2-}, XRD line broadening gives a mean diameter of 120 Å.[4] A particle size distribution was derived from TEM micrographs (Figure 6a) for the Fe_2O_3/6.1% SO_4 catalyst using a magnifying eyepiece to estimate mean particle diameters. The result of this measurement is shown in Figure 6b. The particle dimensions in Figure 6b range from 25 to 300 Å, peaking at 125–150 Å, with an average diameter of approximately 140 Å. Using a procedure described in detail elsewhere,[46] SQUID magnetometry data were interpreted assuming a log normal size distribution, giving the size distribution shown in Figure 6c. The distribution obtained from the magnetometry data is in reasonable agreement with the TEM results, peaking at about 110–130 Å, and extending from 70 to 270 Å. The particle dimensions shown in Figure 5b derived from the superparamagnetic Mossbauer relaxation model are similar to both of these results, showing a peak at 80–120 Å, a small percentage of particles in the 0–40-Å size range, and a larger percentage of particles exceeding 118 Å in mean diameter. It should be noted that the size distribution above 118 Å, the critical diameter from eq 2 that corresponds to room temperature, is not really defined by the Mossbauer data other than specifying the percentage of particles exceeding that diameter, since this is the highest temperature at which spectra were obtained in this study. In view of the experimental errors in all of the measurements and deficiencies in the various analysis models used, the agreement on particle size between Mossbauer, magnetic, TEM, and XRD measurements is considered satisfactory. One difference that is notable is the larger percentage of particles <40 Å in diameter detected by the Mossbauer measurement. This suggests higher sensitivity for the Mossbauer method for these smaller particles, which could be related to the resolution of the TEM (~1 nm) and the long normal distribution model used for the SQUID data.

It is of interest to work backwards and use the derived size distributions to try to derive the Mossbauer spectra. This is done for the Fe_2O_3 on carbon black catalyst in Figure 7. Here we have used the size distribution of Figure 4, the Mossbauer parameters of bulk Fe_2O_3, and theoretical expressions for Mossbauer relaxation spectra[33,43] to derive the room temperature spectrum of this catalyst. The theoretical spectrum is seen to compare rather well to the experimental spectrum (Figure 7).

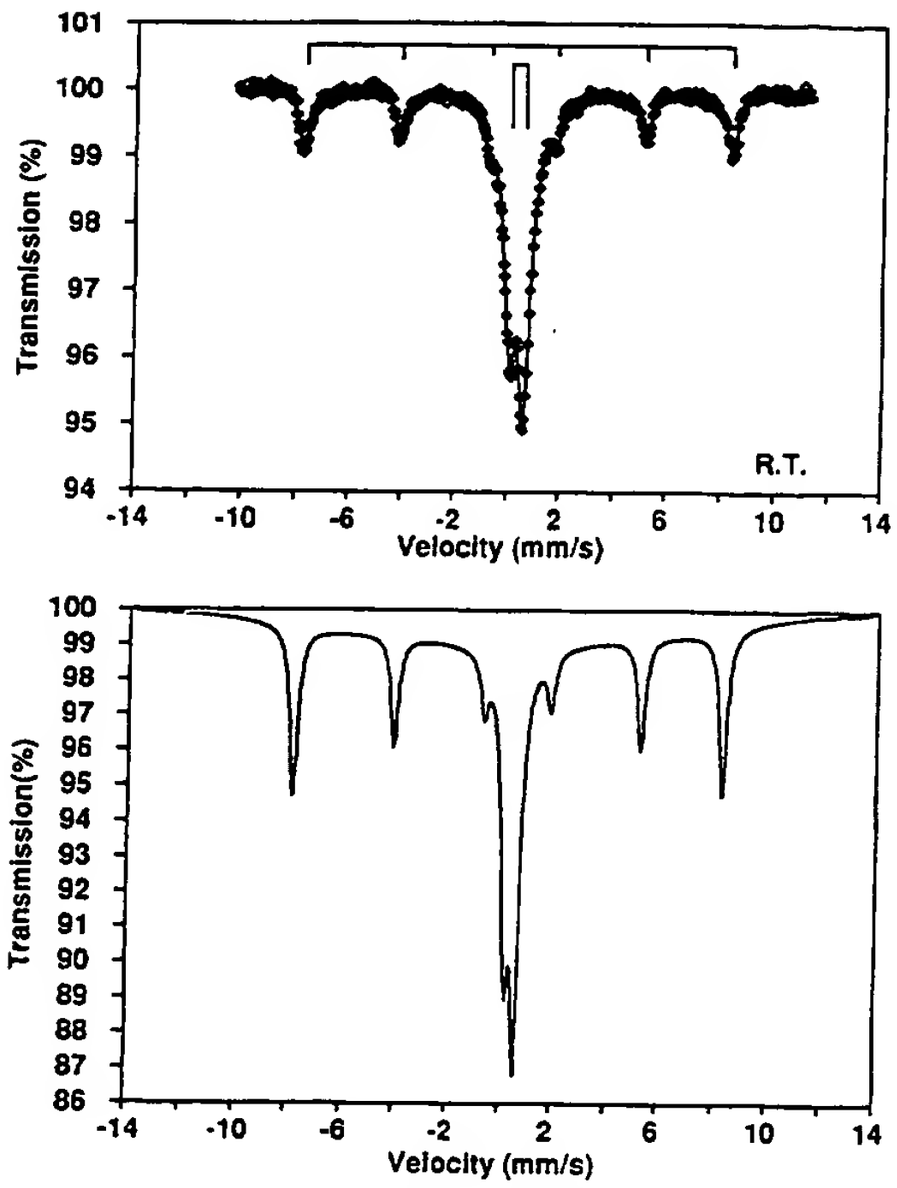

Figure 7. Experimental spectrum of Fe_2O_3 on carbon black and its simulated spectrum using the size distribution from Figure 4.

2. XAFS Spectroscopy Results. The application of XAFS spectroscopy to small particles has been discussed by a number of investigators.[19-21,48,49] In the current article, we will concentrate primarily on the information derived from the radical structure functions obtained by Fourier transformation of the extended X-ray absorption fine structure (EXAFS) region of the XAFS spectra. The radical structure function (RSF) for bulk α-Fe_2O_3 is compared to the radial distribution function obtained from crystallographic data in Figure 8. As discussed in detail elsewhere,[50,51] each peak in the RSF represents the photoelectron backscattering contribution of one or more shells of atoms surrounding the central iron atom absorbing the incident X-rays. These peaks in the RSF are shifted backward slightly (by ~0.5 Å) from the locations of the atomic shells because of phase shifts in the photoelectron wave functions.[50,51] The peaks due to oxygen and iron neighbor shells are appropriately labeled in Figure 8.

In Figures 9 and 10, the RSF of a number of as-prepared or as-dispersed catalysts are compared to the RSF of bulk hematite (α-Fe_2O_3) and bulk goethite (α-FeOOH). It is seen that the principal peaks from different neighbor shells for the catalysts occur at approximately the same distances from the central iron atom as those for the standards. However, it is evident that the amplitudes of the iron shell

(47) Richardson, J. T.; Desai, P. *J. Catal.* 1976, *42*, 294.

(48) Greegor, R. B.; Lytle, F. W. *J. Catal.* 1980, *63*, 476–486.

(49) Zhao, J.; Montano, P. A. *Phys. Rev. B* 1989, *40*, 3401.

(50) Lee, P. A.; Citrin, P. H.; Eisenberger, P.; Kincaid, B. M. *Rev. Mod. Phys.* 1981, *53*, 769–806.

(51) Stern, E. A. Theory of EXAFS. In *X-Ray Absorption*; Knoningsberger, D. C., Prins, R., Eds.; John Wiley & Sons: New York, 1988; pp 3–52.

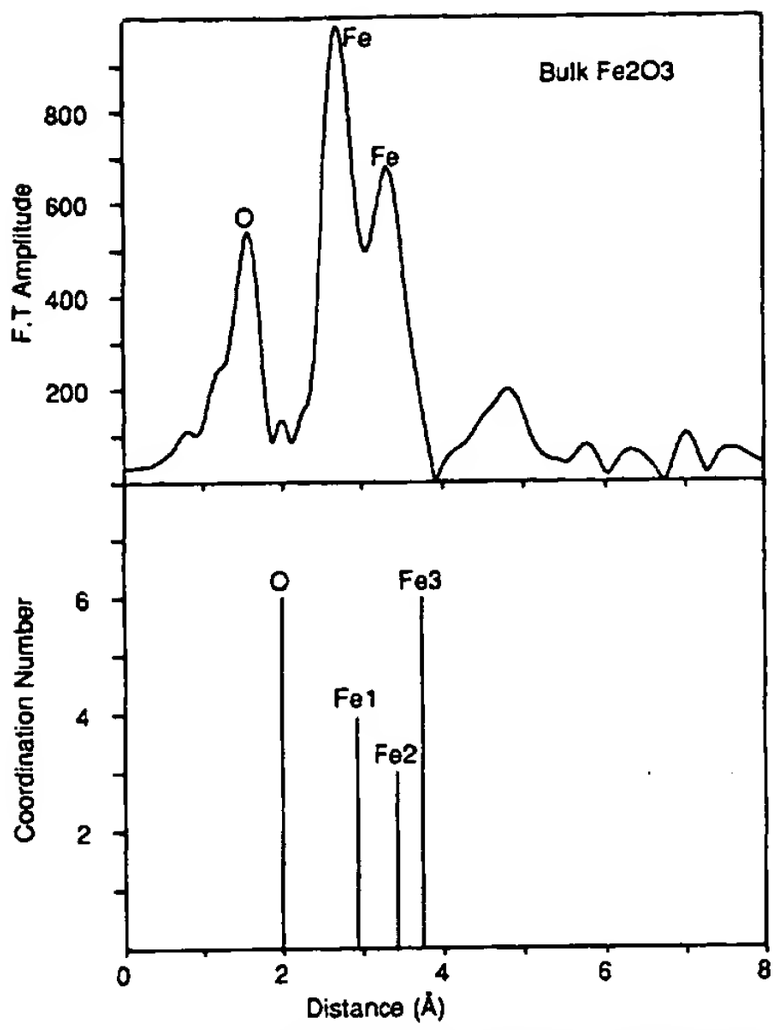

Figure 8. Comparison of the RSF on bulk hematite to the radial distribution function.

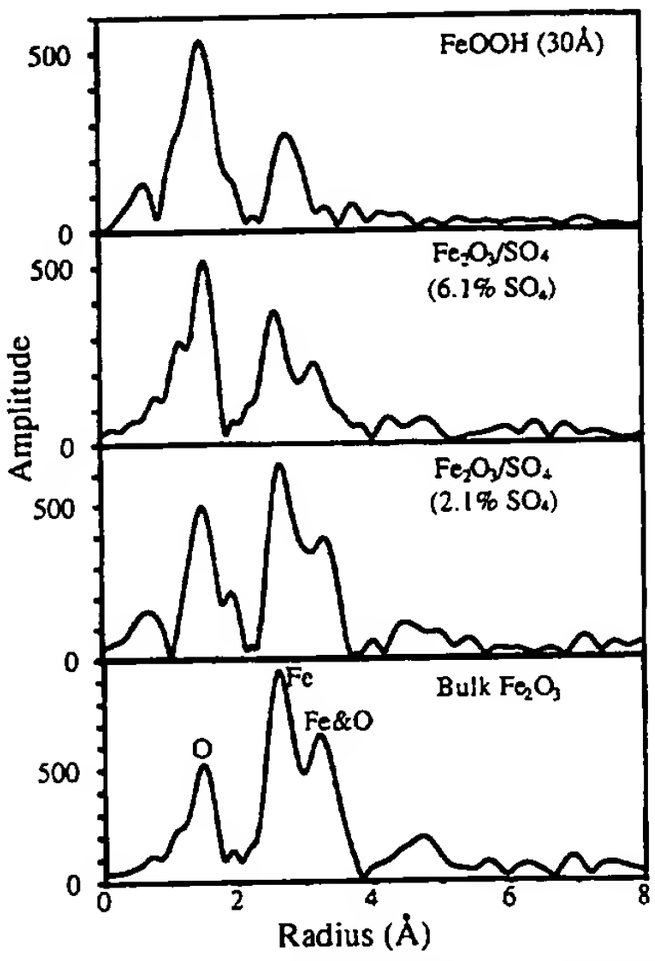

Figure 9. Comparison of the RSF of bulk hematite to those of several catalysts.

peaks of the catalyst RSF are significantly reduced relative to those of the standards. This effect is particularly pronounced for the chemically treated coals. It is noted that, for the chemically impregnated Wyodak coal, a sulfur shoulder due to the pyrite in the coal is observed just beyond the oxygen shell peak (Figure 10c). The cation-exchanged lignite (Figure 10b) was demineralized prior to treatment and therefore contains little or no pyrite.

By performing a least-squares analysis of the back transform of a peak or set of peaks in the RSF, both the interatomic distances and coordination numbers of the various neighbor shells can be determined.[50,51] Typical back transforms are shown in Figure 11, which compares the back transforms of the three principal iron shell peaks (approximately 2.0–4.0 Å in the RSF) for bulk hematite and an Fe_2O_3/SO_4^{2-} catalyst. The variables in the least-squares fits for the catalyst samples are the three interatomic distances and the coordination numbers for the

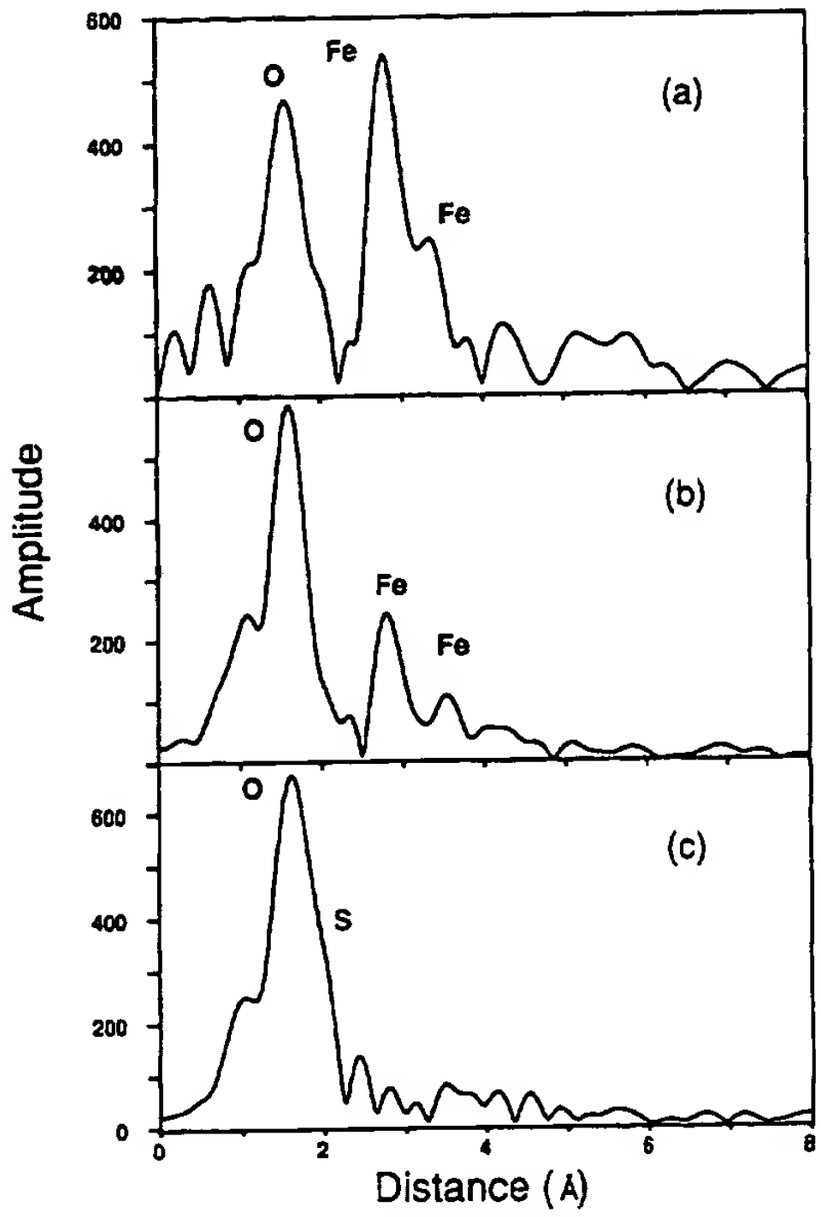

Figure 10. Radial structure functions of bulk goethite (a), a cation-exchanged lignite (b), and chemically impregnated Wyodak coal (c).

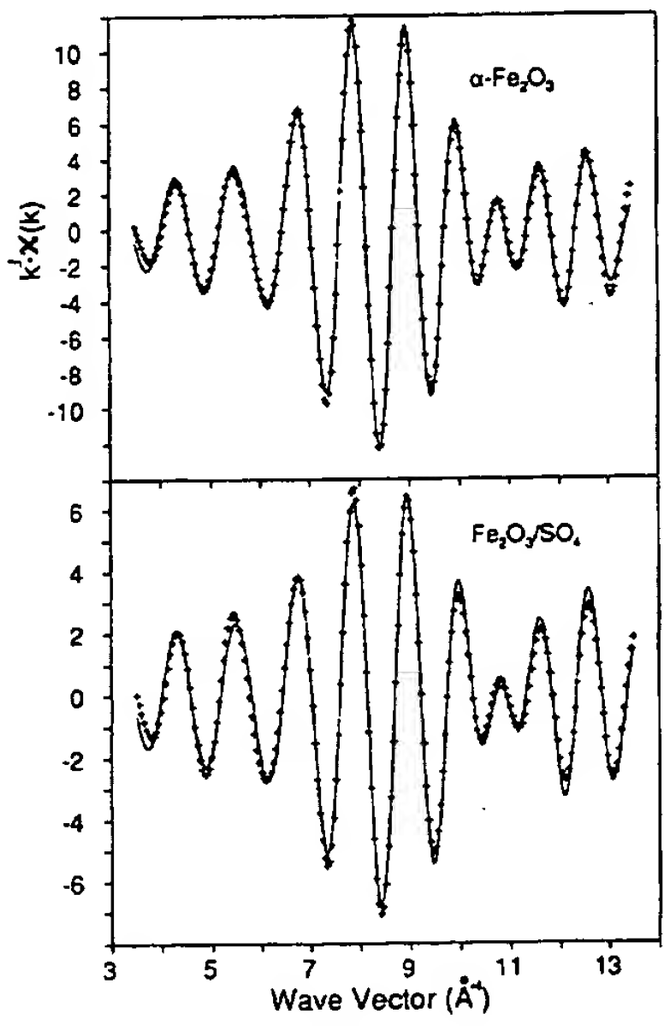

Figure 11. Least-squares fitting of the iron shell peaks for α-Fe_2O_3 and a sulfated Fe_2O_3/SO_4 catalyst.

three iron neighbor shells, using the hematite back transform as the standard amplitude envelope. Similarly, the back transforms of selected shells in the RSF of catalysts which appeared to exhibit an FeOOH structure were least-squares analyzed using goethite as a standard. The interatomic distances and coordination numbers of the neighbor shells out to a distance of approximately 4.0 Å are given for all of the standard iron compounds of interest in Table II.[52] The results obtained by least-squares

(52) Wyckoff, W. R. *Crystal Structures*; Interscience: New York, 1964.

Table II. Coordination Numbers (CN) and Distances of the Iron Neighbor Shells of Various Iron Standards[a]

sample	shell	distance (Å)	CN
hematite, α-Fe_2O_3	Fe–O	⟨2.02⟩	6
	Fe–Fe	2.94	4
	Fe–Fe	3.38	3
	Fe–Fe	3.70	6
geothite, α-FeOOH	Fe–O	⟨2.08⟩	6
	Fe–Fe	3.03	2
	Fe–Fe	3.39	6
pyrrhotite, $Fe_{1-x}S$	Fe–S	2.34–2.63	6
	Fe–Fe	2.95	2
	Fe–Fe	3.10	2
	Fe–Fe	3.53	2
	Fe–Fe	3.73	2
pyrite, FeS_2	Fe–S	2.26	6
	Fe–S	3.43	6
	Fe–S	3.62	2
	Fe–Fe	3.82	12

[a] The value in ⟨ ⟩ denotes the average distance.

Table III. Interatomic Distances and Coordination Numbers (CN) of Various As-Prepared and As-Dispersed Iron-Based Catalysts

sample	shell	distance (Å) (±0.02 Å)	CN (±20%)
Fe_2O_3/SO_4 (6.1% SO_2)	Fe–O	1.99	5.7
	Fe–Fe	2.93	1.8
	Fe–Fe	3.33	1.3
	Fe–Fe	3.66	1.6
Fe_2O_3/SO_4 (2.1% SO_4)	Fe–O	2.02	5.0
	Fe–Fe	2.93	2.3
	Fe–Fe	3.35	1.9
	Fe–Fe	3.67	2.6
Fe_2O_3 on carbon	Fe–O	1.97	5.7
	Fe–Fe	2.94	2.1
	Fe–Fe	3.37	1.3
	Fe–Fe	3.69	2.4
30 Å iron oxide	Fe–O	1.99	5.7
	Fe–Fe	3.04	2.3
	Fe–Fe	3.14	0.8
α-FeOOH/SO_4	Fe–O	1.94	6.7
	Fe–Fe	3.05	1.7
	Fe–Fe	3.38	3.0
cation-exchanged lignite $Fe(OOCCH_3)_2$ soln	Fe–O	1.97	4.4
	Fe–Fe	3.03	0.8
	Fe–Fe	3.39	0.5
	Fe–Fe	3.87	1.4
cation-exchanged lignite $FeCl_2$ soln	Fe–O	1.98	6.4
	Fe–Fe	2.78	
chemically impregnated Wyodak coal	Fe–O	1.92	5.6
	Fe–S	2.26	2.0
chemically impregnated Blind Canyon coal	Fe–O	2.06	5.0

analyses of the back transforms of the principal RSF peaks for the as-prepared or as-dispersed iron catalysts are given in Table III. As noted above, the iron added chemically to coal appears to assume an FeOOH type of structure. It is also seen that the finest Fe_2O_3 sample, the 30-Å Nanocat catalyst from Mach I, appears to have become hydrated, as its interatomic distances are more similar to α-FeOOH than to α-Fe_2O_3. The interatomic distances and coordination numbers determined for the nearest-neighbor oxygen shell are generally within the standard deviations of the bulk compound values for all specimens. However, while the interatomic distances of the iron neighbor shells determined for the catalysts are within the standard deviations of those of the standards, the coordination numbers are significantly decreased from those of the bulk compounds. One possible origin of this effect is the fact that the iron atoms on or near the surfaces of these ultrafine particles have on average fewer iron neighbors in these shells.

Greegor and Lytle[48] have observed similar results in their EXAFS studies of supported metal catalysts and have developed a model relating average coordination numbers for different neighbor shells to the size and shape of the catalyst particles. We have developed a similar model to do the same thing with catalysts of the Fe_2O_3 structure. This is illustrated in Figure 12 where the ratio of the coordination numbers for the iron shells in the catalyst to those for bulk Fe_2O_3 are plotted as a function of the particle radius for approximately spherical particles. For the catalysts of Table III, this figure gives the following results for particle diameters: Fe_2O_3/SO_4^{2-} (6.1% SO_4), 12 Å; Fe_2O_3/SO_4^{2-} (2.1% SO_4), 18 Å; Fe_2O_3 on carbon black, 14 Å. These particle diameters are clearly much less than those obtained by other techniques. A partial explanation is that some of the particles are somewhat tabular in shape; the smallest particle dimensions would presumably be predominantly perpendicular to the paper in Figure 6a, for example. Greegor and Lytle proposed that the Pt and Os catalyst particles they investigated were disk shaped in order to explain particle size underestimation in their study.[48] In the current case, however, *most* of the particles would have to extremely thin (a few monolayers) for this to be the only origin of size underestimation. Zhao and Montano[49] have pointed out that surface effects can cause a significant reduction in the electron mean free path. This can also cause a substantial reduction in the apparent coordination numbers derived from the standard back transform analysis. We believe that this is the primary origin of the smaller than expected coordination numbers given in Table III.

3. Structure of Reacted Catalysts. A more limited study has been made of the structure of highly dispersed iron-based catalysts after DCL or related hydrotreatment reactions. Typical Mossbauer spectra obtained from solid DCL residues are shown in Figure 13 and a summary of all Mossbauer data obtained from such samples is given in Table IV. For the most part, these samples were derived from DCL experiments conducted at the University of Pittsburgh using either sulfated Fe_2O_3[4] or iron pentacarbonyl ($Fe(CO)_5$).[2] It is seen that the iron in the residues is present primarily in the form of pyrrhotite ($Fe_{1-x}S$) and superparamagnetic oxides. Minor amounts of pyrite are present in some samples, presumably remnants of the pyrite originally present in the coal that have not transformed to pyrrhotite.

The superparamagnetic oxides are predominantly ferric, and presumably represent catalyst not yet converted to pyrrhotite by reaction with H_2S. In one case, however, a low sulfur, very low pyrite Blind Canyon coal (Penn State sample bank, DECS-6) was liquefied with a sulfated Fe_2O_3 catalyst, and extracted directly from a stirred autoclave under nitrogen to prevent alteration of the sample. The resulting catalyst form in the solid residue was a superparamagnetic magnetite. When the same liquefaction experiment was carried out with elemental sulfur added (S/Fe = 2), essentially all of the added catalyst was converted to pyrrhotite.

It should be noted that the pyrrhotite, which is the dominant species in most of these samples, is derived both from devolatization of the pyrite in the coal and sulfidation of the added catalyst. It is seen that the pyrrhotite spectrum consists of several magnetic hyperfine components, reflecting the fact that Fe atoms that are exchange-coupled to different numbers of Fe second nearest

Table IV. Mössbauer Results for the Iron Contained in IOM after DCL Reaction[a]

sample	phase	H	LS	QS	% Fe	vacancy
Ill#6/Maya + Fe_2O_3/SO_4	pyrite		0.26	0.72	3	
	pyrrhotite	301	0.73	0.01	25	0.11
	pyrrhotite	280	0.71	0.5	39	
	pyrrhotite	261	0.71	0.07	33	
Ill#6/Maya, no catalyst	pyrite		0.26	0.60	4	
	pyrrhotite	293	0.69	0.05	38	0.07
		266	0.71	0.05	46	
		243	0.59	0.17	12	
Ill#6/Maya, $Fe(CO)_5$	para/sp Fe^{3+} Ox.		0.43	0.59	32	
	pyrrhotite	295	0.70	0.06	26	0.08
	pyrrhotite	267	0.70	0.06	31	
	pyrrhotite	234	0.57	0.13	11	
Ill#6/Maya, $Fe(CO)_5$ + Mo as $Mo(CO_6)$	para/sp Fe^{3+} Ox.		0.40	0.61	25	
	pyrrhotite	300	0.69	0.04	22	0.10
	pyrrhotite	275	0.70	0.06	39	
	pyrrhotite	245	0.61	0.14	15	
Ill#6/Maya, $Fe(CO)_5$ + Mo as naphthanate	para/sp Fe^{3+} Ox.		0.46	0.52	39	
	pyrrhotite	297	0.68	0.06	31	0.05
	pyrrhotite	266	0.69	0.05	22	
		234	0.55	0.16	7	
Wyodak/Maya, no catalyst	para/sp Fe^{3+} Ox.		0.41	0.60	31	
	pyrrhotite	297	0.69	0.04	27	0.08
	pyrrhotite	262	0.72	0.02	31	
	pyrrhotite	226	0.57	0.15	10	
Wyodak/Maya + $Fe(CO)_5$	para/sp Fe^{3+} Ox.		0.48	0.42	40	
	para/sp Fe^{3+} Ox.		0.40	1.02	10	
	Fe oxide	449	0.58		5	
	Fe oxide	417	0.69		4	
	pyrrhotite	295	0.67	0.04	17	0.07
	pyrrhotite	253	0.65	0.02	13	
	pyrrhotite	222	0.61	0.11	10	
Up. Frp./Maya, no catalyst	Fe^{3+} Ox.		0.35	0.65	30	
	pyrrhotite	290	0.67	0.05	26	0.08
	pyrrhotite	259	0.58	0.12	41	
Up. Frp./Maya + $Fe(CO)_5$	Fe^{3+} Ox.		0.34	0.64	21	
	pyrrhotite	293	0.70	0.05	32	0.07
	pyrrhotite	265	0.68	0.07	47	
Ill#6 + Fe_2O_3/SO_4 (3.4% SO_4)	pyrite		0.3	0.75	7	
	pyrrhotite	302	0.74	−0.01	28	0.10
	pyrrhotite	281	0.72	0.06	35	
	pyrrhotite	261	0.71	0.06	30	
Ill#6 + Fe_2O_3/SO_4 (6.1% SO_4)	pyrite		0.31	0.65	2	
	pyrrhotite	295	0.70	0.04	32	0.09
	pyrrhotite	274	0.72	0.04	41	
	pyrrhotite	257	0.68	0.10	25	
Bl. Can. + Fe_2O_3/SO_4 (1 h)	magnetite	485	0.35		31	
	magnetite	458	0.75		43	
	spm magnetite		0.33	0.42	26	
Bl. Can. + Fe_2O_3/SO_4 (43 min)	magnetite	480	0.28		30	
	magnettite	453	0.71		46	
	spm magnetite		0.37	0.42	24	
Bl. Can. + Fe_2O_3/SO_4 (23 min)	magnetite	482	0.29		29	
	magnetite	455	0.73		42	
	spm magnetite		0.37	0.37	29	
Bl. Can. + Fe_2O_3/SO_4 (5 min)	magnetite	485	0.34		23	
	magnetite	458	0.66		11	
	spm magnetite		0.44	0.40	49	
	spm magnetite		1.01	2.28	18	

[a] The approximate error in the reported values is 5%.

neighbors (nn) exhibit different magnetic hyperfine fields. Since the largest fields will be experienced by those atoms that have no vacancies in the second nn shell, the vacancy content can be determined from

$$P_0 = (1 - x)^{12}$$

$$x = 1 - \exp\{(\ln P_0)/12\} \quad (4)$$

where P_0 is the fraction of iron atoms that exhibits the largest magnetic hyperfine field. It is seen in Table IV that the vacancy concentration, x, for these samples varies from about 5 to 11%.

4. In Situ XAFS Spectroscopy Studies. One of the advantages of XAFS spectroscopy in catalysis research is that it is possible to carry out in situ studies of catalyst reactions at elevated temperatures in user-selected environments in a reasonable reaction time. We have completed some initial studies of the reactions of iron-based catalysts in a hydrogen donor solvent, hexahydropyrene (HHP), at 100–320 °C in the presence of added elemental sulfur. The sulfur to iron ratio was approximately 2.

The RSF obtained for the Mach I 30-Å Fe_2O_3 catalyst and for a sulfated Fe_2O_3 (3.4% SO_4) catalyst are shown in Figures 14 and 15. The results obtained by back transform analysis for the interatomic distances and coordination numbers of various atomic neighbor shells are summarized in Table V. It appears that the 30-Å Fe_2O_3 specimen

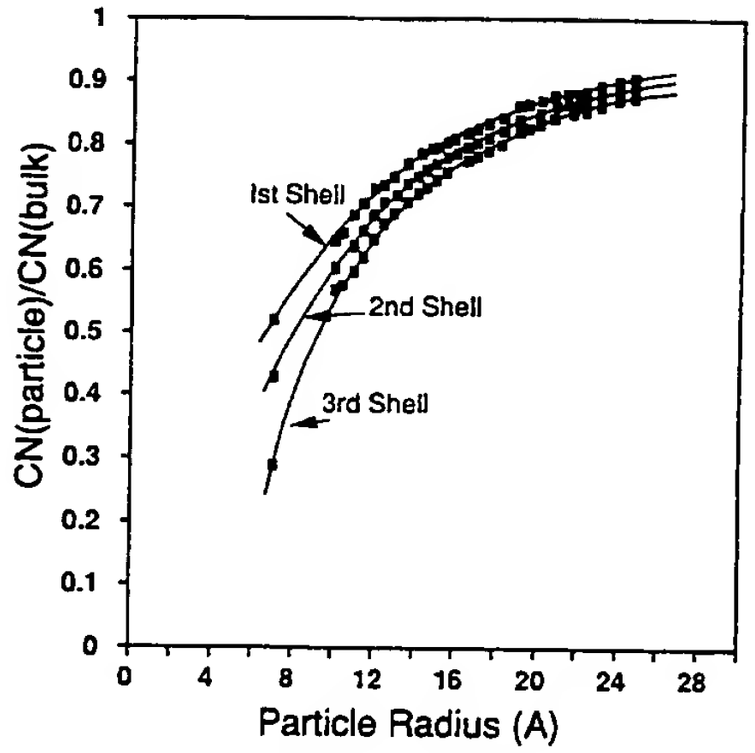

Figure 12. Ratio of coordination numbers of iron neighbor shells for small Fe_2O_3 particles to those for bulk Fe_2O_3 as a function of particle radius.

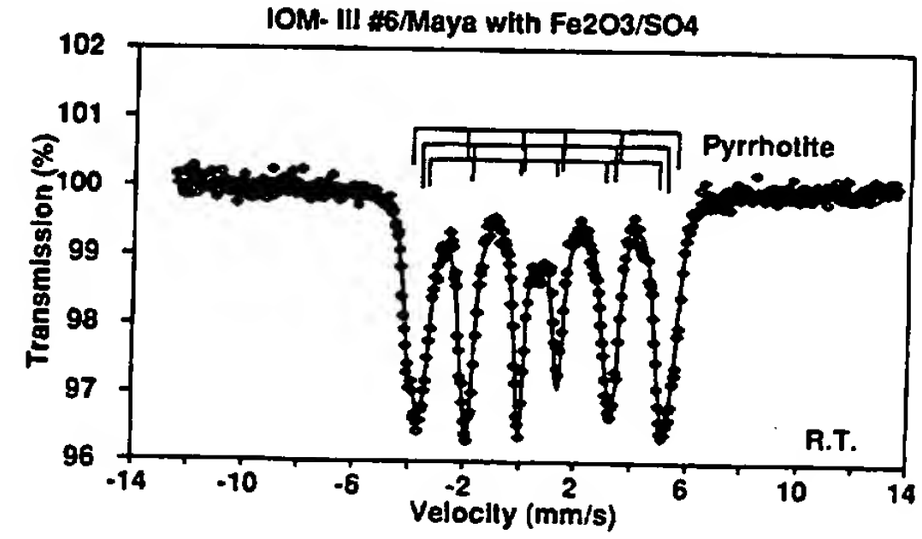

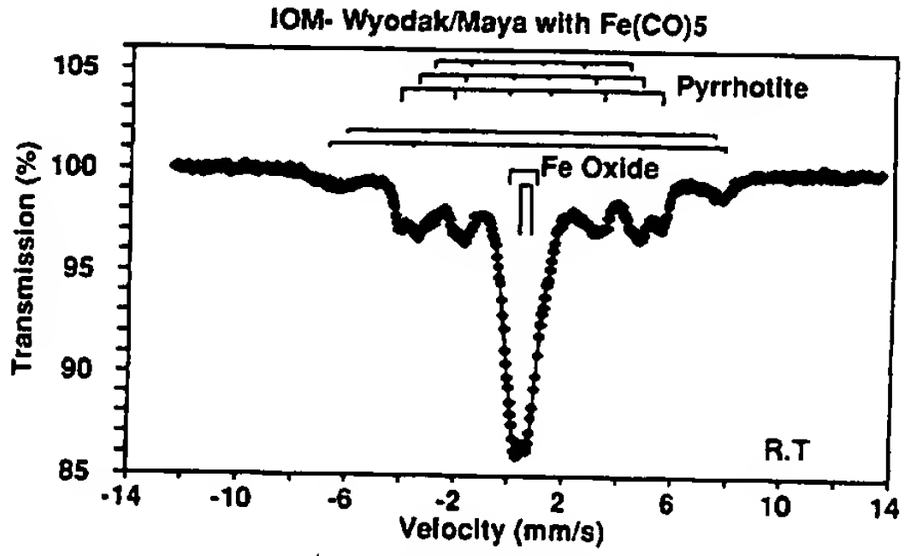

Figure 13. Mössbauer spectra illustrating the case where all pyrite and added catalyst is converted to pyrrhotite (top), and where only half of the added catalyst is converted to pyrrhotite, (bottom).

undergoes some reaction with S even at room temperature, as evidenced by a small peak in the RSF corresponding to a S shell at 2.39 Å. The transformation of the 30-Å Fe_2O_3 catalyst to pyrrhotite is clearly well in progress at as low a temperature as 110 °C, is about 50% completed at 180 °C, and is quickly completed (<~5 min) at 320 °C. With regard to the time scale of the in situ experiment, each spectrum required about 45 min to complete, and two scans were run at each temperature. The sulfated Fe_2O_3 catalyst, which is much larger in mean particle size (>100 Å) does not exhibit any transformation below 250 °C, and requires 90–100 min to completely transform to pyrrhotite at 320 °C.

Summary and Conclusions

Mossbauer spectroscopy, XAFS spectroscopy, and a number of complementary techniques have been used to

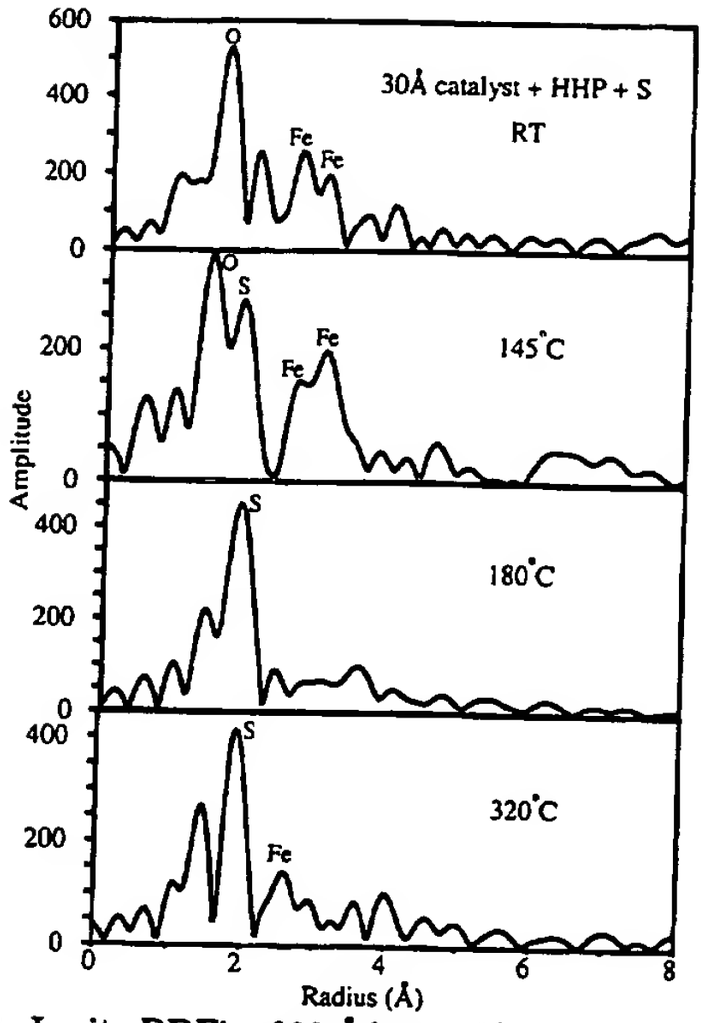

Figure 14. In situ RDF's of 30-Å iron oxide catalyst mixed with hexahydropyrene at indicated temperatures.

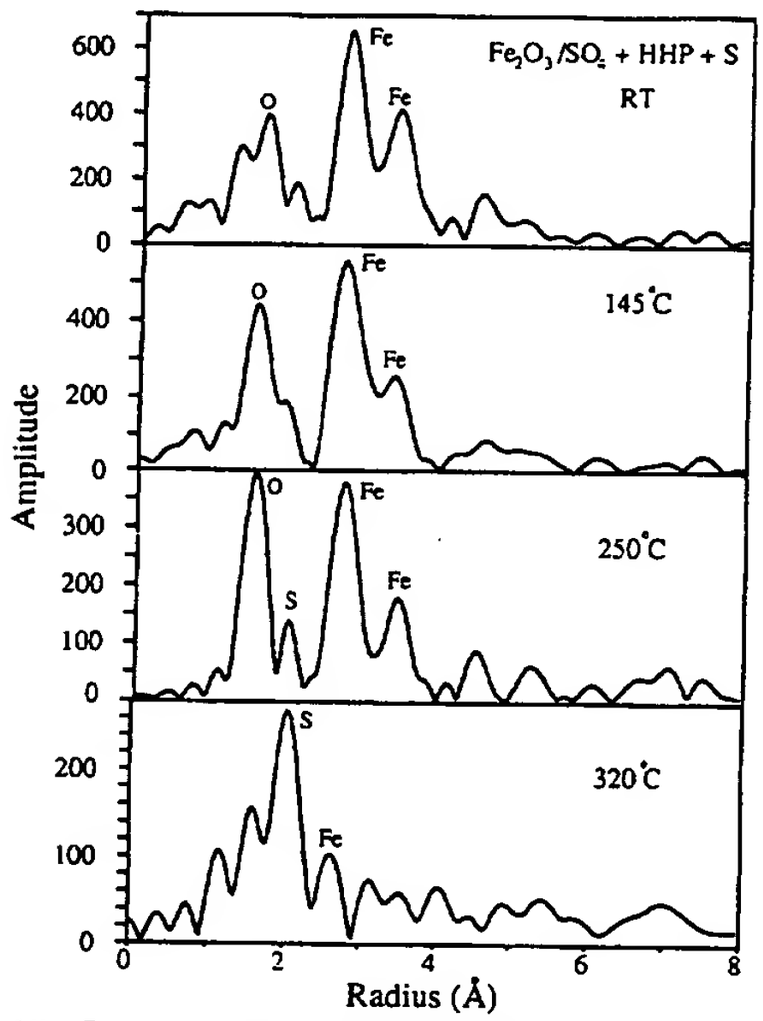

Figure 15. In situ RDF's of Fe_2O_3/SO_4 catalyst mixed with hexahydropyrene plus elemental sulfur at indicated temperatures.

investigate the structure and size dispersion of a variety of ultrafine iron-based DCL catalysts. In the as-prepared state, iron that was chemically incorporated into the coal exhibited an FeOOH structure, while iron catalysts prepared separately had the Fe_2O_3 structure.

The Mossbauer spectra of the as-prepared catalysts exhibited pronounced superparamagnetic relaxation effects. It was shown that the relaxation spectra could be analyzed to yield particle volumes and that such analyses of spectra obtained at several temperatures provide a size distribution for the catalyst particles. While a number of approximations are involved in this interpretation, comparison of the Mossbauer-determined size distributions to size information obtained by SQUID magnetometry, STEM, and XRD gave reasonable agreement.

Radial structure functions (RSF) derived from the XAFS spectra of the as-prepared catalysts confirmed the

Table V. Coordination Numbers and Distances of the Iron Neighbor Shells Determined from in Situ XAFS Spectra

sample	shell	distance (Å) (±0.02 Å)	CN (±20%)
30-Å iron oxide catalyst plus S in HHP at			
room temperature	Fe–O	1.98	4.6
	Fe–S(?)	2.39	1.3
	Fe–Fe	2.99	0.7
	Fe–Fe	3.41	0.9
145 °C	Fe–O	1.95	4.1
	Fe–S	2.38	1.3
	Fe–Fe	3.05	0.9
	Fe–Fe	3.53	0.5
180 °C	Fe–O	2.09	3.9
	Fe–S	2.46	3.7
320 C, then cooled to room	Fe–S	2.46	6.5
temp	Fe–Fe	3.02	5.5
Fe_2O_3/SO_4 (2.1% SO_4) plus S in HHP at			
room temp	Fe–O	1.96	6.6
	Fe–Fe	3.00	2.3
	Fe–Fe	3.42	1.5
	Fe–Fe	3.74	3.0
250 °C	Fe–O	1.92	4.2
	Fe–S	2.41	0.9
	Fe–Fe	3.00	1.7
	Fe–Fe	3.40	0.4
	Fe–Fe	3.78	0.6
320 °C	Fe–S	2.46	5.4
	Fe–Fe	*a*	*a*
room temp after 320 °C	Fe–S	2.47	7.0
	Fe–Fe	2.99	6.0

[a] Signal too weak for analysis.

Mossbauer structural identifications and also exhibited significant size effects. While the interatomic distances determined from the RSF were essentially the same as those of the bulk phases, the coordination numbers of the iron neighbor shells were significantly decreased and scaled with particle size. The origin of this effect is believed to be twofold: (i) iron atoms on or near the surface of fine particles have fewer iron neighbors at distances of 3–4 Å; and (ii) the electron mean free path is decreased for very small particles, leading to an apparent decrease in coordination numbers of more distant neighbor shells.

During DCL, the highly dispersed ferric iron rapidly reacts with H_2S to form pyrrhotite ($Fe_{1-x}S$). If insufficient sulfur is present in the reactor to convert all of the iron to pyrrhotite, the remainder is left in the form of a superparamagnetic oxide, but may transform to a mixed ferric–ferrous state, such as magnetite. An in situ XAFS study of the reactions of ultrafine Fe_2O_3 catalysts in a hydrogen donor solvent in the presence of elemental sulfur showed that conversion of a 30-Å catalyst to pyrrhotite proceeded fairly rapidly at 110–180 °C, while the transformation of an Fe_2O_3 catalyst of larger particle size (>100 Å) proceeded somewhat sluggishly at 250–320 °C.

Future research on this topic will include additional in situ XAFS spectroscopy studies of catalyst reactions under simulated liquefaction conditions, in situ Mossbauer studies of catalyst reactions, and investigation of ultrafine, bimetallic iron-based catalysts.

Acknowledgment. This research was supported by the U.S. Department of Energy under DOE Contract No. DE-FC22-90PC90029 as part of the cooperative research program of the Consortium for Fossil Fuel Liquefaction Science. The XAFS spectroscopy measurements were carried out at the National Synchrotron Light Source at Brookhaven National Laboratory, which is also supported by the U.S. Department of Energy. We thank Dr. Bernard M. Kosowski of Mach I, Inc. for providing us with samples. We also thank Dr. Malvina Farcasiu of the Pittsburgh Energy Technology Center for providing us with samples and for a number of useful suggestions.